

# The Number Density of $0.6 < z < 1.7$ Mg II Systems from CORALS: Observational Biases at Intermediate Redshift<sup>1</sup>

Sara L. Ellison

*University of Victoria, Dept. Physics & Astronomy, Elliott Building, 3800 Finnerty Rd,  
Victoria, V8P 1A1, British Columbia, Canada*

sarae@uvic.ca

Chris W. Churchill

*Department of Astronomy, New Mexico State University, 1320 Frenger Mall, Las Cruces,  
New Mexico, USA*

cwc@nmsu.edu

Samantha A. Rix<sup>2</sup>, Max Pettini

*Institute of Astronomy, Cambridge, Madingley Rd, Cambridge, CB3 0HA, UK*

srix@ing.iac.es, pettini@ast.cam.ac.uk

## ABSTRACT

The goal of the Complete Optical and Radio Absorption Line System (CORALS) survey is to quantify the potential impact on QSO absorber statistics from dust in intervening galaxies. Dust may introduce a selection bias in surveys which are based on magnitude limited QSO samples, leading to an underestimate of absorber number density,  $n(z)$ . Here we present the results of the second phase of the CORALS survey which extends our previous work on  $z > 1.8$  damped Lyman  $\alpha$  systems (DLAs) to search for strong metal line systems (candidate DLAs) in the range  $0.6 < z < 1.7$ . We have identified 47 Mg II systems with rest frame equivalent widths  $EW(\text{Mg II}\lambda 2796) > 0.3 \text{ \AA}$  in our sample of 75 radio-selected quasars. The total redshift path covered by the survey is  $\Delta z = 35.2, 58.2$  and  $63.8$  for  $EW(\text{Mg II}\lambda 2796) > 0.3, 0.6$  and  $1.0 \text{ \AA}$  thresholds respectively ( $5 \sigma$ ). Our principal and most robust result is that the  $n(z)$  of low redshift Mg II systems determined for the CORALS survey is in excellent agreement with that of

---

<sup>2</sup>Current address: Isaac Newton Group, Apartado 321, 38700 Santa Cruz de La Palma, Spain

optically-selected, magnitude limited QSO samples. We use empirically determined Mg II equivalent width statistics to estimate the likely number of DLAs in this sample. The statistically inferred number density of DLAs,  $n(z) = 0.16_{-0.06}^{+0.08}$ , is consistent with other low redshift samples, although the large  $1\sigma$  error bars permit up to a factor of 2.5 more DLAs in CORALS. However, confirmation of the DLA candidates, precise evaluation of their  $n(z)$  and measurement of their H I column densities awaits UV observations with the *Hubble Space Telescope*. Finally, we report an excess of intermediate redshift Mg II systems observed towards bright QSOs which could be due to a lensing amplification bias. However, there is also evidence that this excess could simply be due to more sensitive EW detection limits towards brighter QSOs. We also emphasize that absorber statistics determined from magnitude limited surveys reach a steady value if the completeness limit is significantly fainter than the fiducial value of the quasar luminosity function.

*Subject headings:* ISM:general, galaxies:high-redshift, quasars:absorption lines, dust, extinction

## 1. Introduction

Modern instrumentation has provided us with two techniques capable of identifying high redshift ( $z \gtrsim 3$ ) galaxies in relatively large numbers. Direct detection of star-forming galaxies via deep multi-color imaging employs broad band photometry in filters which span characteristic continuum breaks (e.g. Steidel et al. 1996; Lowenthal et al. 1997; Giavalisco 2002; Adelberger et al. 2004). A complementary approach uses spectroscopy of distant QSOs whose lines of sight penetrate intervening gas clouds associated with galaxies and the intergalactic medium (e.g. Wolfe et al. 1986). These two techniques occupy different astrophysical niches; the former identifies the brightest, most actively star forming galaxies at early epochs (e.g. Sawicki & Yee 1998; Shapley et al. 2001; Nandra et al. 2002) whereas the latter selects galaxies via their absorption cross section of neutral hydrogen. In particular, damped Ly $\alpha$  systems (DLAs) are often proclaimed to be ‘unbiased’ tracers of galaxy evolution and are expected to provide a fair census of neutral gas at all redshifts. However, despite the lack of Malmquist bias, DLA statistics are susceptible to other possible

---

<sup>1</sup>These data were obtained from the 3.6-m on La Silla (70.A-0006), UT3 on Paranal (69.A-0053,71.A-0011), the WHT on La Palma (W/2002A/10) and the Baade telescope at Las Campanas

selection effects. For example, dust in intervening galaxies may cause significant extinction of background sources which would make dusty absorbers more difficult to detect in optical surveys. Obfuscation of background QSOs is also theoretically supported (Ostriker & Heisler 1984; Fall & Pei 1993; Masci & Webster 1995 ) and often invoked as an explanation for observed trends such as the anti-correlation between the neutral hydrogen column density,  $N(\text{H I})$ , and metallicity (e.g. Prantzos & Boissier 2000). However, Murphy & Liske (2004) have recently determined  $E(B - V)$  values of less than 0.01 magnitudes (assuming an SMC extinction curve) for DLAs in the Sloan Digital Sky Survey. Selection against evolved galaxies may also be responsible for the lack of metallicity evolution (Pettini et al. 1999) in DLAs. If it is shown that dust obscuration is not an important effect, then we must appeal to alternative explanations for these observed trends.

In order to specifically address the issue of dust biasing in DLA surveys, we have designed the Complete Optical and Radio Absorption Line System survey (CORALS). CORALS is based on a sample of radio-selected quasars (Jackson et al. 2002) with complete optical identifications. The key here is that QSO selection was executed at a wavelength immune to extinction, and yet optical counterparts have been identified for every target. The high redshift ( $z_{\text{abs}} > 1.8$ ) results of CORALS I (Ellison et al. 2001) indicate that the effect of dust bias at this redshift is relatively minor, although a larger radio selected sample would be desirable to improve the statistics. These results do not indicate that dust is entirely absent in high redshift DLAs. On the contrary, there is evidence from a number of observations including chemical abundances, (Pettini et al. 1997), QSO colors and spectral indices (Pei, Fall & Bechtold 1991; Outram et al. 2001) and Lyman break galaxies (Sawicki & Yee 1998; Shapley et al. 2003) that dust is present at these early times. Apparently extinction in the majority of gas-rich galaxies at  $z > 2$  has only a minor effect on the statistics of QSO surveys with optical magnitude limits  $V \lesssim 20$ .

At low redshift, however, the story may be quite different. The most prominent sources of dust today are the envelopes of evolved, cool, stars which can be distributed into the ISM by winds. However, in order to explain the large amounts of dust already present at high redshift (e.g. Priddey & McMahon 2001; Bertoldi et al. 2003), additional sources such as supernovae (Morgan & Edmunds 2003; Dunne et al. 2003) and AGN (Elvis, Marengo & Karovska 2002) have been proposed, although our understanding of dust formation at any epoch remains sketchy. Regardless of the source of dust, it seems plausible that stars (and possibly AGN) must be well established before grains can be distributed in the ISM. The epoch around  $z = 2 - 3$  is emerging as an important formative stage in the universe's history, with both star formation and QSO space density declining steeply after this time (Madau et al. 1996; Shaver et al. 1996). Moreover, Dickinson et al. (2003) and Rudnick et al. (2003) have shown that this is the epoch when stellar mass sees marked evolution; only

about 5 – 10% of galactic stellar mass is apparently in place before a redshift of 2.5, but 50 – 75% at  $z \sim 1$ . Models of chemical evolution also predict a more serious dust bias at low redshift (e.g. Masci & Webster 1999; Churches, Nelson & Edmunds 2004). Moreover, our only direct evidence of spectral dust features seen in absorption is at  $z < 1$ . Malhotra (1997) found evidence for the 2175 Å absorption feature in a composite of 96 Mg II systems with an average redshift of  $z \sim 1.2$ . The same feature has also recently been identified in a  $z \sim 0.5$  DLA (Junkkarinen et al. 2004) and in a  $z = 0.8$  lensing galaxy (Motta et al. 2002). No evidence for this extinction feature has been found at higher redshift (Fall, Pei & McMahon 1989). This clearly highlights the need to quantify the dust bias at  $z < 1.5$ .

In order to extend the CORALS I survey to lower redshifts where dust bias may be more pronounced, we have executed a complementary follow-up survey. In this paper, we present the results of this survey which targets Mg II absorption systems primarily in the range  $0.6 < z < 1.7$ , once again utilizing an optically complete radio-selected sample of QSOs. A survey for strong Mg II systems is a stepping stone towards the quantification of dust bias in DLAs, which form a subset of the systems discovered here. Future follow-up observations with the Hubble Space Telescope (*HST*) will allow us to confirm the H I column densities of the candidate DLAs discovered by CORALS and determine unbiased statistics for this population at intermediate redshifts. We describe the design of the survey (§2), the observations (§3) and tabulate the absorption systems identified (§4). We present our absorption line statistics in §5 and §6. Discussion and conclusions can be found in §7 and §8 respectively.

## 2. Survey Design

The original CORALS I sample selected all QSOs with  $z_{\text{em}} > 2.2$  from the Parkes 0.25 Jy flat spectrum sample of Jackson et al. (2002). We imposed this lower redshift bound because our survey was limited to DLAs at  $z_{\text{abs}} > 1.8$ . For DLAs at lower redshifts, the Ly $\alpha$  line occurs at a wavelength where the throughput of most spectrographs drops significantly and at  $z_{\text{abs}} \lesssim 1.6$  Ly $\alpha$  falls bluewards of the atmospheric cut-off, completely precluding ground-based detection. Since Ly $\alpha$  observations with the *HST* for an optically complete sample are not feasible due to its limited aperture, we adopted an alternative strategy for our low redshift CORALS survey (CORALS II). Based on the approach of Rao & Turnshek (2000, RT00), we selected systems with large rest equivalent widths (EWs) of Mg II  $\lambda\lambda 2796, 2803$  and Fe II  $\lambda 2600$  as candidate DLAs. These metal lines can be efficiently observed in ground-based optical spectra over the range  $0.6 \lesssim z \lesssim 1.8$ . We can assess the severity of dust bias in previous surveys by determining the number of Mg II systems, as well as the statistically

inferred number of DLAs.

In order to extend the CORALS survey to lower redshifts using Mg II, it is necessary to re-define the original QSO sample so that it is optimized for this task. Moreover, the observations from CORALS I are not suitable for the identification of moderate redshift Mg II for two reasons. First, we must target the continuum redward of Ly $\alpha$  whereas the wavelength range of CORALS I spectra often covers only the Ly $\alpha$  forest. Second, the CORALS I spectra were of insufficient resolution and signal-to-noise ratio (S/N) for consistent identification of the Mg II doublet (a minimum resolving power  $R \equiv \lambda/\Delta\lambda \simeq 900$  is required in order to resolve the Mg II  $\lambda\lambda 2796, 2803$  doublet). Thus, for the present CORALS II survey we have selected all sources with  $1.80 < z_{\text{em}} < 2.55$  from the parent sample of 0.25 Jy Parkes flat spectrum QSOs. The high systemic redshift cut-off was selected so that even for the lowest redshift Mg II systems (typically  $z_{\text{abs}} \sim 0.6$ ) the Mg II  $\lambda\lambda 2796, 2803$  Å doublet was always located redwards of Ly $\alpha$  emission. Although the corresponding lower systemic redshift cut-off could have consequently extended to  $z_{\text{em}} = 0.6$ , this would have yielded an unmanageable number of survey sightlines given observational facilities at our disposal. The lower redshift cut-off was therefore set to  $z_{\text{em}} = 1.80$ , resulting in a sample of 75 QSOs.

### 3. Observations and Data Reduction

Spectra were obtained with a variety of instruments on 4- to 8-m telescopes: ISIS (William Herschel Telescope), EFOSC2 (ESO 3.6-m), the Boller & Chivens (B&C; Magellan-Baade) and FORS1 (VLT UT3). All observations executed at the VLT were obtained in service mode. A summary of the observation dates and instrumental setups is given in Table 1. In Table 2 we list the observed QSOs, exposure times, magnitudes and redshifts. The transparency conditions were generally clear to photometric and seeing ranged from approximately 0.5 to 1.5 arcsec. For EFOSC2, B&C and ISIS, the slit was aligned at the parallactic angle at the start of each observation; for FORS1 we used the atmospheric dispersion corrector.

All but two of the 75 QSOs in our sample have been observed, availability of telescope time precluding the observation of two of our faintest targets. Although the main objective of this survey is to achieve optical completeness, the exclusion of two sightlines is extremely unlikely to affect our number density statistics.

The data were reduced using standard IRAF<sup>2</sup> routines to execute the usual corrections

---

<sup>2</sup>IRAF is written and supported by the IRAF programming group at the National Optical Astronomy

for flat fields and bias structure. We note that EFOSC2 has a very narrow overscan strip ( $\sim 6$  pixels) that could not be used, so that only the average bias frame was subtracted. Special attention was paid to the flat fielding of the ISIS spectra where significant structure is introduced by the dichroic response, by vignetting on the new large format red arm CCD (applicable to the October 2002 data), and by interference patterns at red wavelengths. The spectra were optimally extracted and wavelength calibrated using HeAr (EFOSC2), CuAr+CuNe (ISIS), HeArNe (B&C) or HeNeArCdHg (FORS1) lamps. In the case of FORS1 and EFOSC2, the instrument flexure is minimal and arcs were obtained only at the start and the end of each night. For ISIS and the B&C spectrographs, arcs were taken before or after each science target. Although the observing conditions did not allow precise absolute flux determination, the intrinsic continuum shape has been recovered by flux calibrating with spectrophotometric standards taken through the night. The calibrated spectra were then combined and shifted to a vacuum heliocentric reference frame. Finally, a correction for Galactic interstellar reddening was applied assuming the empirical selective extinction function of Cardelli, Clayton & Mathis (1989) and  $E(B-V)$  values taken from the DIRBE extinction maps of Schlegel, Finkbeiner & Davis (1998) with an assumed  $R_V=3.1$ . In Figure 1 we present examples of the spectra obtained for this project from each telescope utilized.

#### 4. Mg II System Doublet Identification

The search for Mg II  $\lambda\lambda$  2796, 2803 Å doublets was undertaken using an automated search algorithm based on the technique originally designed for identification of absorption lines in the *HST* QSO key project spectra (Schneider et al. 1993). We have refined this technique; full details can be found in Churchill et al (2000a). Here we give only a brief qualitative summary of the steps involved.

For each flux spectrum, we calculated an EW and an EW uncertainty spectrum. The EW uncertainty spectrum provides a running detection limit as a function of wavelength (e.g., Schneider et al. 1993; Churchill et al. 1999). These spectra are produced by assuming an unresolved line centered on each pixel with weighting of neighbouring pixels by the appropriate instrumental spread function. Using these spectra, we ran an automated routine to objectively locate candidate Mg II doublets. During this automated process, a preliminary measurement of the equivalent widths and the Mg II doublet ratio is computed, again assuming unresolved absorption features.

The objectively determined candidate doublet list is then visually inspected using the

flux spectra to ascertain which are *bona fide* Mg II doublets. Many candidates were corroborated by the detection of one or several Fe II lines and the Mg I  $\lambda 2853$  line. Following visual inspection, roughly 10% of the candidates were discarded. We also visually inspected the flux spectra to search for Mg II candidates that may have been missed in the automated search. We found no candidates missed by the search algorithm.

We then interactively fitted Gaussian profiles to the absorption lines using a  $\chi^2$  minimization routine to determine the final EWs and redshifts (line centers), and their uncertainties (Churchill et al. 2000a). For unresolved lines, the Gaussian width was automatically held at the instrumental spread function width. In the few cases of highly resolved lines, multiple Gaussians were used to determine the EWs. The systems were again inspected to confirm that the redshifts of the  $\lambda 2796$  and  $\lambda 2803$  lines were consistent within  $1 \sigma$  and that they had physically meaningful doublet ratios within the uncertainties. For each system, we then performed Gaussian fitting on statistically significant Mg I and Fe II transitions, or computed the  $3 \sigma$  EW limit for an unresolved feature from the EW uncertainty spectrum at the expected location of the line. The full list of Mg II systems and their Mg II  $\lambda 2796$  and Fe II  $\lambda 2600$  EWs is given in Table 3.

## 5. Survey Coverage

The advantage of our line detection algorithm is that it computes the effective detection limit at each resolution element, allowing us to easily calculate the survey coverage as a function of EW threshold. The redshift path density for a given EW threshold,  $g(EW_{min}, z_i)$ , is the number of lines of sight in our survey at which a Mg II doublet of rest equivalent width  $EW_{min}$  at redshift  $z_i$  could have been detected:

$$g(EW_{min}, z_i) = \sum_j H(z_i - z_j^{min}) H(z_j^{max} - z_i) H[EW_{min} - w_{min}^j(z_i)] \quad (1)$$

for  $j$  QSOs in the survey.  $H$  is the Heaviside step function,  $z^{min,max}$  correspond to the minimum and maximum redshifts at which Mg II were searched and  $w_{min}^j(z_i)$  is the calculated EW detection limit at  $z_i$ . In Figure 2 we plot  $g(EW_{min}, z_i)$  for our survey, adopting three EW thresholds:  $EW_{min} > 0.3, 0.6$  and  $1.0 \text{ \AA}$  ( $5 \sigma$ ). This figure illustrates that for the range  $0.7 < z < 1.4$  we are almost 100% complete (except at  $z \sim 1.18$  due to a gap in the wavelength coverage of the ISIS spectra) for  $EW_{min}=0.6, 1.0 \text{ \AA}$  and about 50% complete for a threshold EW limit of  $0.3 \text{ \AA}$ .

The total redshift path,  $\Delta z$ , of the survey is given by

$$\Delta z = \int_0^\infty g(EW_{min}, z_i) dz \quad (2)$$

In Figure 3 we plot the total redshift path as a function of EW limit for both 3 and 5  $\sigma$  detection limits. Corresponding values of  $\Delta z$  are listed in Table 4 for various combinations of  $EW_{min}$  and detection significance as a supplement to the information in Figure 3. Table 4 additionally includes redshift coverage values for simultaneous detection of Mg II  $\lambda 2796$  and Fe II  $\lambda 2600$ ; this point will be discussed in §7.1.

## 6. Results

### 6.1. Mg II Number Density

The number density of absorbers per unit redshift,  $n(z)$ , is computed for a given mean absorption redshift by dividing the number of systems by  $\Delta z$ . In Table 5 we present the values of  $\Delta z$  and number of absorbers for CORALS II, as well as the large surveys of Steidel & Sargent (1992, SS92) and RT00. Figure 4 compares the  $n(z)$  determined for CORALS II and other surveys as a function of redshift. We use the statistics of SS92 for  $EW > 0.3 \text{ \AA}$  and preliminary statistics from the Sloan Digital Sky Survey (SDSS) Early Data Release ( $EW > 1.0 \text{ \AA}$ , Nestor et al. 2003a). Since CORALS is a smaller survey than the SDSS or SS92 and evolution in the number density is very mild over the redshift range that we cover, we combine our  $n(z)$  statistics into one redshift bin. The results in Figure 4 demonstrate an excellent agreement between the CORALS value of  $n(z)$  and that determined from the SDSS survey of Nestor et al. The SDSS results for the intermediate EW threshold of  $0.6 \text{ \AA}$  (Nestor et al. in preparation) are also in excellent agreement with the CORALS value. In the lower EW range,  $EW > 0.3 \text{ \AA}$ , there is marginal evidence for a higher number density (at most a factor of two) in the CORALS sample compared with SS92. If this is interpreted within the framework of a dust bias, we would conclude that the weakest Mg II systems are more prone to extinction than high EW systems. This seems unlikely given that a) the lowest EW Mg II systems are likely to be associated with the outer regions of galaxies (e.g. Churchill et al. 2000b; Ellison et al. 2004) and b) strong Mg II systems statistically trace gas with higher metallicities than weak systems (Nestor et al. 2003b). In any case, Figure 4 illustrates the main result of this survey: previous magnitude limited surveys have not under-estimated the number density of Mg II systems in the range  $0.6 < z < 1.6$ .



## 6.2. The Impact of Lensing Amplification Bias

Although the principal focus of the CORALS survey has been the quantification of dust bias, we consider here also the potential effect of gravitational lensing. The possibility that an amplification bias can skew distant source counts has been discussed extensively in the literature (e.g. Turner 1980; Schneider 1987; Hamana et al. 1997). Amongst others, Bartelmann & Loeb (1996), Smette et al. (1997) and Perna, Loeb & Bartelmann (1997) have discussed the specific case of amplification bias in QSO absorption system surveys. These papers describe the dual effect of magnification of the background source and deflection of the sightline from the central part of the lensing galaxy. However, since the observational spotlight has focussed in large part on the detection of *high redshift* DLAs, little concern has been directed towards this possible bias, since lensing becomes less efficient as the redshift of the intervening galaxy approaches that of the QSO. Only in the last few years have large numbers of low redshift DLAs been discovered and studied, renewing interest in the potential effect of the amplification bias.

Le Brun et al. (2000) studied 7 QSOs with  $z < 1$  DLAs. In no case did they find multiple images and they therefore concluded that amplification of the sources was at most 0.3 magnitudes. However, these authors also noted that these QSOs are fainter than those in many low redshift DLA surveys and are therefore less likely to be affected by amplification bias. Using a large sample of 2dF QSOs, Menard & Péroux (2003, MP03) have reported the first convincing evidence of amplification bias by showing that bright QSOs ( $B \lesssim 19.5$ ) are more likely to have intervening Mg II absorbers than fainter ones. However, Péroux et al. (2004) have also shown that gravitational lensing bias has no demonstrable effect on the total column density of intervening H I gas and the mass fraction of neutral gas in low redshift absorbers.

In Figure 5 we reproduce an analogous plot to Figure 5 of MP03 and confirm qualitatively their result: there is an excess of bright QSOs with absorbers. Excluding from our least squares fit the brightest magnitude bin which has a large error because of small number statistics, we find a slope of  $-0.3$ . This gradient is somewhat shallower than the value  $-0.66$  found by MP03, although these authors also show that the slope is quite sensitive to the band selected.

In order to understand this dependence on magnitude, it is important to consider the shape of the optical luminosity function (OLF) of QSOs. If the quasar OLF were a single power law, then absorber number statistics should be independent of survey depth, *even in the presence of dust or lensing bias*. A bias due to dust or lensing would alter the  $n(z)$  determined, with a severity dictated by the steepness of the LF, but one would not observe a varying effect as a function of completeness magnitude. However, at all redshifts the quasar

OLF is well modelled by a double power law with a steep index at bright magnitudes and a considerably shallower slope at fainter magnitudes, the turnover depending on the QSO redshift e.g. (Boyle et al. 2000; although see Hunt et al. 2004 for evidence of evolution in the faint end slope at high redshift). It is the transition between ‘bright’ and ‘faint’ QSOs that causes the magnitude dependent effect seen in Figure 5 (and in Figure 5 of MP03).

The negative slope of the fit in Figure 5 indicates that gravitational lensing bias dominates over extinction effects for bright QSOs with intermediate redshift absorbers, as predicted by Perna et al. (1997). However, the wavelength dependent nature of this effect, which is more apparent in red filters (MP03), indicates that dust also makes a contribution. In theory, we can disentangle the effects of dust and lensing by looking at the ratio of QSOs with and without intervening absorbers (as shown in Figure 5) as a function of radio luminosity, since lensing is achromatic, but dust extinction is not. However, unlike the OLF, the quasar radio luminosity function for flat spectrum sources at  $2 < z < 3$  does not show a convincing break (J. Wall, 2004, private communication). We therefore do not expect to find (and indeed do not find) a smooth variation in the ratio of QSO numbers with/without intervening absorbers as a function of radio power.

An alternative explanation for the effect seen in Figure 5 is that higher S/N in the spectra of brighter QSOs facilitates the detection of absorbers towards these sources. In order to test this possibility we have compared the ratio of QSOs with and without intervening absorbers with  $EW \geq 0.6 \text{ \AA}$ . Since we are effectively complete at this EW limit (see Figure 2) imposing this cut should remove any bias due to S/N. The results of this test are shown in Figure 6, where it can be seen that the ‘signature’ of lensing bias seen in Figure 5 vanishes. Clearly, more investigation into gravitational lensing bias with larger QSO samples and with careful quantification of completeness is warranted.

We conclude this section by emphasizing that although the discussion above acknowledges the possible existence of observational biases from dust and lensing, both appear to be relatively minor effects. Moreover, due to the change in the slope of the QSO OLF at  $B \sim 19$ , surveys which have magnitude limits significantly fainter than this fiducial value will not yield absorber statistics which depend on QSO brightness. In fact, the relatively shallow OLF slope at faint magnitudes means that moderate dust (or gravitational lensing bias) will have only a small effect and will not yield number densities significantly different from complete surveys such as CORALS.

## 7. Discussion

### 7.1. DLA Statistics

The ultimate aim of this work is to quantify the obscuration bias associated with DLAs, which form a subset of the strong Mg II absorbers identified here. Although we can not make definitive statements concerning DLA statistics until *HST* observations are in hand, we can speculate upon their number density based on the selection statistics of previous surveys. RT00 have shown that low redshift DLAs can be efficiently pre-selected for UV follow-up based on the EWs of strong metal lines. Specifically, they found in their sample of 87 Mg II systems that 50% of absorbers with  $\text{EW}(\text{Fe II } \lambda 2600, \text{Mg II } \lambda 2796) > 0.5 \text{ \AA}$  were confirmed to be DLAs based on *HST* spectroscopy. Recently, Péroux et al (2004) have investigated whether this pre-selection introduces a bias into DLA surveys, but found no convincing evidence that this is the case. In the absence of direct information on the  $N(\text{H I})$  of our Mg II absorbers, we therefore adopt the RT00 pre-selection as an indication of DLA statistics.

Our survey has been designed specifically with this pre-selection in mind. In Figure 7 we show the  $g(z)$  of our sample if we include the additional criterion of Fe II  $\lambda 2600$  coverage. Figure 7 is therefore analogous to Figure 2 except that the minimum EW thresholds now apply to both transitions. A comparison of the two figures shows that we achieve simultaneous coverage of these two metal lines for the majority of sightlines. There is a small ( $\Delta z \sim 0.1$ ) gap in coverage at the lowest redshift end which is unavoidable, simply because the rest wavelength of Fe II is bluer than that of Mg II. There is a second small dip in  $g(z)$  at  $1.3 < z_{\text{abs}} < 1.4$  caused by the gap in CCD coverage in the ISIS instrument (there is a corresponding gap for Mg II at  $z_{\text{abs}} \sim 1.18$ ).

In Figure 8 we show the Mg II and Fe II rest frame EWs for every system in our catalogue (Table 3). In addition we plot the Mg I  $\lambda 2852$  EW as a function of Mg II  $\lambda 2796$  EW; RT00 find that all systems with  $\text{EW}(\text{Mg I } \lambda 2852) > 0.7 \text{ \AA}$  are confirmed to be DLAs. Based on Mg II and Fe II alone, we have 14 good DLA candidates, six of which have  $\text{EW}(\text{Mg I } \lambda 2852) > 0.7 \text{ \AA}$ . According to the results of RT00, we would statistically expect 50% of the 14 candidates to be confirmed as DLAs. We can re-calculate the redshift path incorporating Fe II coverage for a given sigma and EW limit in order to calculate  $n(z)$  for the DLAs; these values are given in Table 4.

We have calculated  $n_{\text{DLA}}(z)$  for DLAs by assuming 7 absorption systems in the range  $0.6 < z_{\text{abs}} < 1.6$  and  $\Delta z = 44.62$  (at 5 sigma significance for a  $0.5 \text{ \AA}$  detection), i.e.  $n(z) = 0.16_{-0.06}^{+0.08}$ . The average absorption redshift of the 14 systems with  $\text{EW}(\text{Mg II } \lambda 2796, \text{Fe II } \lambda 2600) > 0.5 \text{ \AA}$  is  $\langle z \rangle = 1.07$ . In Figure 9 we compare this value with previous DLA surveys at high

(Storrie-Lombardi & Wolfe 2000) and low redshifts (RT00). We additionally include the  $z = 0$  number density from Rosenberg & Schneider (2003) which is in good agreement with other local H I studies such as those by Ryan-Weber et al. (2003) and Zwaan et al. (2002). We conclude that the number density of DLAs expected statistically in our sample is consistent with that from previous surveys based on optically selected samples. However, the small number of inferred systems (which needs to be confirmed with UV spectroscopy) leads to large ( $1\sigma$ ) error bars which permit up to a factor of 2.5 difference with previous DLA surveys.

## 7.2. Average Metallicity of DLA Systems

One of the outstanding questions concerning DLAs is why their metallicities remain low ( $\lesssim 1/10Z_{\odot}$ ), even at low-to-intermediate redshifts (e.g. Pettini et al. 1999). It has previously been speculated (e.g. Pei & Fall 1995; Pettini et al. 1999; Prantzos & Boissier 2000; Churches et al. 2004) that dust bias could cause an artificial cut-off in the observed metallicities. Akerman et al. (in preparation) have found that this is not the case at high redshift: the mean metallicity of  $z > 2$  DLAs from CORALS I is in agreement with that in optically selected samples.

We can attempt a crude comparison of metallicities between DLA candidates in our survey and those in an optically selected sample, namely the SDSS. Nestor et al. (2003b) have found that the mean metallicity (based on  $[Zn/H]$  in composite spectra) of their SDSS Mg II sample was higher for larger EW Mg II systems. We therefore compare the median Mg II EW from our survey with that determined from the SDSS sample. Nestor et al (2003a) provisionally fit the EW distribution with an exponential of the form

$$n(EW) = n_0 e^{-EW/EW^*} \quad (3)$$

with a value of  $EW^* = 0.7 \text{ \AA}$ . This value is in very good agreement with the previous determination of  $EW^*$  by SS92, who also give an alternative formulation of

$$n(EW) = CEW^{-\delta} \quad (4)$$

with a value of  $\delta = 1.65$ , which we adopt here. From Eq. (4) we determine a median value of the EW that depends on the minimum and maximum cut-offs adopted:

$$2EW_{median}^{1-\delta} = EW_{max}^{1-\delta} + EW_{min}^{1-\delta} \quad (5)$$

Applying to our CORALS II sample the minimum EW cut-off of Nestor et al. (2003b),  $EW=1 \text{ \AA}$ , we measure a value of  $EW_{median} = 1.50 \text{ \AA}$ , in good agreement with the theoretical median of  $1.57 \text{ \AA}$  determined from Eq. (5), adopting the maximum  $EW = 3 \text{ \AA}$  found in our sample. This good correspondence between the median equivalent widths of the CORALS II and SDSS Mg II samples further suggests that the typical metallicity of low redshift CORALS absorbers is unlikely to be significantly higher than that of absorbers from optically selected QSO samples. However, only a fraction of DLAs will have sufficiently large  $N(\text{H I})$  and high metallicities to cause severe obscuration; Cen et al. (2003) estimate a fraction of  $\sim 10\%$ . Since our statistics are based on only 7 DLAs, such a small sample of candidate DLAs is unlikely to sample the full metallicity distribution function.

## 8. Conclusions

We have performed a new survey for Mg II absorption systems in the range  $0.6 < z_{\text{abs}} < 1.7$  from a radio selected quasar sample with complete optical identifications. The strongest of these Mg II systems, particularly those with accompanying Fe II absorption, are good candidates for DLAs. We have used these data to quantify, for the first time, the effect of dust bias on the completeness of optically selected surveys for low redshift Mg II systems.

Our most robust result is that the number density of Mg II systems is in excellent agreement with previous studies based on optically selected QSOs. Combined with the result of our high redshift survey (Ellison et al. 2001), we have not yet found any evidence for a statistically significant dust bias in absorption system surveys over the range  $0.5 \lesssim z_{\text{abs}} \lesssim 3.5$ .

At bright magnitudes ( $B \lesssim 19$ ) we observe a mild excess of QSOs with intervening low redshift absorbers which may be due to gravitational lensing bias. However, this excess is not present when only absorbers with  $EW > 0.6 \text{ \AA}$  are included, indicating that incompleteness may be at least partly responsible. Our discussion of gravitational lensing bias and its dependence on the shape of the QSO OLF highlights an important conclusion for absorption line surveys: an optical completeness fainter than the fiducial point in the OLF ( $B \sim 19$ ) will not yield number densities that are dependent on QSO magnitude.

Using the empirical pre-selection technique of Rao & Turnshek (2000) we have attempted to estimate the number of DLAs in our sample and hence their number density. By assuming that 50% of absorbers with  $EW(\text{Fe II } \lambda 2600, \text{Mg II } \lambda 2796) > 0.5 \text{ \AA}$  are statistically likely to be confirmed as DLAs, we determine the DLA number density at  $\langle z \rangle = 1.07$  to be  $n(z) = 0.16^{+0.08}_{-0.06}$ . This is consistent with previous estimates of  $n(z)$  at this redshift, but the large  $1\sigma$  error bars permit up to a factor of 2.5 difference. The number density relies both

on an empirical pre-selection and relatively small number statistics and should therefore be confirmed with follow-up observations of the Ly $\alpha$  transition.

Finally, the median equivalent width of the CORALS II Mg II systems is in good agreement with that of optically selected absorbers in the SDSS. This is suggestive of consistent metallicities between the two samples, since Nestor et al. (2003b) find that larger EW Mg II systems have higher metallicities in their SDSS composites.

The next important step is to measure the  $N(\text{H I})$  of our candidate DLAs. This will permit us to calculate the neutral gas mass density of our complete low redshift sample and allow us to determine metallicities with ground-based telescopes. Once we have determined the  $N(\text{H I})$  of these systems, there are several foreseeable follow-up projects, such as 21 cm absorption measurements which will yield spin temperatures for the absorbing galaxies. The few measurements of spin temperature that have already been obtained hint at some intriguing trends (e.g. Kanekar & Chengalur 2003), but there is an absence of data points in the important range  $0.7 < z < 1.7$ . Such follow-up programs will build on the uniqueness of CORALS and exploit fully the benefits of this radio-selected sample.

We are extremely grateful to Remi Cabanac who performed the March 2001 EFOSC2 run for us and to Paul Green and John Silverman for the opportunity to obtain several spectra at the Baade telescope at Las Campanas Observatory. We thank Dan Nestor for providing the SDSS determinations of  $n(z)$  in advance of publication and Arif Babul and Jon Willis for useful discussions on gravitational lensing. SAR acknowledges PPARC for a PhD studentship. This work made use of the NASA Extragalactic Database (NED).

## REFERENCES

- Adelberger, K. L., Steidel, C. C., Shapley, A. E., Hunt, M. P., Erb, D. K., Reddy, N. A., & Pettini, M. 2004, *ApJ*, 607, 226
- Bartelmann, M., & Loeb, A. 1996, *ApJ*, 457, 529
- Bertoldi, F., Carilli, C. L., Cox, P., Fan, X., Strauss, M. A., Beelen, A., Omont, A., & Zylka, R. 2003, *A&A*, 406, 55
- Boyle, B. J., Shanks, T., Croom, S. M., Smith, R. J., Miller, L., Loaring, N., & Heymans, C. 2000, *MNRAS*, 317, 1014
- Cardelli, J. A., Clayton, G. C., & Mathis, J. S. 1989, *ApJ*, 345, 245

- Cen, R., Ostriker, J. P., Prochaska, J., Wolfe, A. M., 2003, *ApJ*, 598, 741
- Churches, D. K., Nelson, A. H., & Edmunds, M. G. 2004, *MNRAS*, 347, 1234
- Churchill, C. W. 2001, *ApJ*, 560, 92
- Churchill, C. W., Mellon, R. R., Charlton, J. C., Jannuzi, B. T., Kirhakos, S., Steidel, C. C., & Schneider, D. P. 2000a, *ApJS*, 130, 91
- Churchill, C. W., Mellon, R. R., Charlton, J. C., Jannuzi, B. T., Kirhakos, S., Steidel, C. C., Schneider, D. P., et al. 2000b, *ApJ*, 543, 577
- Churchill, C. W., Rigby, J R., Charlton, J. C., & Vogt, S. S. 1999, *ApJS*, 120, 51
- Dickinson, M., Papovich, C., Ferguson, H. C., & Budavari, T. 2003, *ApJ*, 587, 25
- Dunne, L., Eales, S., Ivison, R., Morgan, H., & Edmunds, M. 2003, *Nature*, 424, 285
- Ellison, S. L., Ibata, R., Pettini, M., Lewis, G. F., Aracil, B., Petitjean, P., & Srianand, R. 2004, *A&A*, 414, 79
- Ellison, S. L., Yan, L., Hook, I., Pettini, M., Wall, J., & Shaver, P. 2001, *A&A*, 379, 393
- Elvis, M., Marengo, M., & Karovska, M. 2002, *ApJ*, 567, 107
- Fall, S. M., & Pei, Y. 1993, *ApJ*, 402, 479
- Fall, S. M., Pei, Y., & McMahon, R. G. 1989, *ApJ*, 341, L5
- Giavalisco, M., 2002, *ARA&A*, 40, 579
- Hamana, T., Futamase, K., Futamase, T., & Kasai, M. 1997, *MNRAS*, 287, 341
- Hunt, M. P., Steidel, C. C., Adelberger, K. L., & Shapley, A. E. 2004, *ApJ*, 605, 625
- Jackson, C. A., Wall, J. V., Shaver, P. A., Kellermann, K. I., Hook, I. M., & Hawkins, M. R. S. 2002, *A&A*, 386, 97
- Junkkarinen, V., et al., 2004, *ApJ*, submitted
- Kanekar, N., & Chengalur, J.N. 2003, *A&A*, 399, 857
- Le Brun, V., Smette, A., Surdej, J., & Claeskens, J.-F. 2000, *A&A*, 363, 837
- Lowenthal, J. D., Koo, D. C., Guzman, R., Gallego, J., Phillips, A. C., Faber, S. M., Vogt, N. P., Illingworth, G. D., & Gronwall, C. 1997, *ApJ*, 481, 673

- Madau, P., Ferguson, H. C., Dickinson, M. E., Giavalisco, M., Steidel, C. C., & Fruchter, A. 1996, *MNRAS*, 283, 1388
- Malhotra, S. 1997, *ApJ*, 488, L101
- Masci, F. J., & Webster, R. L. 1995, *PASA*, 12, 146
- Masci, F. J., & Webster, R. L. 1999, *MNRAS*, 305, 937
- Menard, B., & Péroux, C. 2003, *A&A*, 410, 33
- Morgan, H. L., & Edmunds, M. G. 2003, *MNRAS*, 343, 427
- Motta, V., Mediavilla, E., Munoz, J. A., Falco, E., Kochanek, C. S., Arribas, S., Garcia-Lorenzo, B., Oscoz, A., & Serra-Ricart, M. 2002, *ApJ*, 574, 719
- Murphy, M. T., & Liske, J., 2004, *MNRAS* submitted, astro-ph/0405472
- Nandra, K., Mushotzky, R. F., Arnaud, K., Steidel, C. C., Adelberger, K. L., Gardner, J. P., Teplitz, H. I., & Windhorst, R. A. 2002, *ApJ*, 576, 625
- Nestor, D. B., Rao, S. M., Turnshek, D. A., & Furst, E. 2003a, *ASSL Conference Proceedings*, 281, 133
- Nestor, D. B., Rao, S. M., Turnshek, D. A., & Vanden Berk, D. 2003b, *ApJ*, 595, L5
- Ostriker, J. P., & Heisler, J. 1984, *ApJ*, 278, 1
- Outram, P. J., Smith, R. J., Shanks, T., Boyle, B. J., Croom, S. M., Loaring, N. S., & Miller, L. 2001, *MNRAS*, 328, 805
- Pei, Y., Fall, S. M., 1995, *ApJ*, 454, 69
- Pei, Y., Fall, S. M., & Bechtold, J. 1993, *ApJ*, 402, 479
- Perna, R., Loeb, A., & Bartelmann, M. 1997, *ApJ*, 488, 550
- Péroux, C., Deharveng, J.-M., Le Brun, V., Cristiani, S., 2004, *MNRAS*, accepted, astro-ph/0405352
- Pettini, M., Ellison, S. L., Steidel, C. C., & Bowen, D. V. 1999, *ApJ*, 510, 576
- Pettini, M., Shapley, A., Steidel, C., Cuby, J.-G., Dickinson, M., Moorwood, A., Adelberger, K., & Giavalisco, M. 2001, *ApJ*, 554, 981



- Pettini, M., Smith, L. J., King, D. L., & Hunstead, R. W. 1997, *ApJ*, 486, 665
- Prantzos, N., & Boissier, S. 2000, *MNRAS*, 315, 82
- Priddey, R., & McMahon, R. 2001, *MNRAS*, 324, 17
- Rao, S.M., & Turnshek, D.A. 2000, *ApJS*, 130, 1
- Rosenberg, J., & Schneider, S. 2003, *ApJ*, 585, 256
- Rudnick, G., et al. 2003, *ApJ*, 599, 847
- Ryan-Weber, E. V., Webster, R. L., & Staveley-Smith, L. 2003, *MNRAS*, 343, 1195
- Sawicki, M. J., & Yee, H. K. C. 1998, *AJ*, 115, 1329
- Schlegel, D.J., Finkbeiner, D.P., & Davis, M. 1998 *ApJ*, 500, 525
- Schneider, P. 1987, *A&A*, 83, 189
- Schneider, D. P., et al. 1993, *ApJS*, 87, 45
- Shapley, A. E., Steidel, C. C., Adelberger, K. L., Dickinson, M., Giavalisco, M., & Pettini, M. 2001, *ApJ*, 562, 95
- Shapley, A. E., Steidel, C. C., Pettini, M., & Adelberger, K. L. 2003, *ApJ*, 588, 65
- Shapley, A. E., Erb, D. K., Pettini, M., Steidel, C. C., & Adelberger, K. L. 2004, *ApJ*, in press (astro-ph/0405187)
- Shaver, P. A., Wall, J. V., Kellermann, K. I., Jackson, C. A., & Hawkins, M. R. S. 1996, *Nature*, 384, 439
- Smette, A., Claeskens, J.-F., & Surdej, J. 1997, *New Astronomy* 2, 53
- Steidel, C. C., Giavalisco, M., Pettini, M., Dickinson, M., Adelberger, K. L. 1996, *ApJL*, 462, L17
- Steidel, C. C. & Sargent, W. L, W. 1992, *ApJS*, 80, 1
- Steidel, C. C., Shapley, A. E., Pettini, M., Adelberger, K. L., Erb, D. K., Reddy, N. A., & Hunt, M. P. 2004, *ApJ*, 604, 534
- Storrie-Lombardi, L., & Wolfe, A. M. 2000, *ApJ* 543, 552
- Turner, E. L. 1980, *ApJ*, 242, L135

Wolfe, A. M., Turnshek, D. A., Smith, H. E., & Cohen, R. D. 1986, ApJS, 61, 249

Zwaan, M., Briggs, F., & Verheijen, M. 2002, ASP Conference Proceedings Vol. 254, 169

Table 1. Observing Journal

Telescope	Instrument	Grating/ Grism	Resolution FWHM ( $\text{\AA}$ )	Wavelength Coverage ( $\text{\AA}$ )	Observing Dates
3.6-m	EFOSC2	# 9	5.5	4730 – 6700	March 12-13 2002
3.6-m	EFOSC2	# 9	5.5	4730 – 6700	Nov. 9-11 2002
WHT	ISIS	R600B	1.9	4430 – 6000	March 17-18 2002
WHT	ISIS	R600R	1.8	6185 – 6970	March 17-18 2002
WHT	ISIS	R600B	1.9	4430 – 6000	Sept. 30 – Oct 3 2002
WHT	ISIS	R600R	1.8	6120 – 7500 <sup>a</sup>	Sept. 30 – Oct 3 2002
UT3	FORS1	600V	5.1	4830 – 7200	Aug. 4-5 2002
Baade	B&C	600/5000	4.1	4140 – 7300	Jan. 26 2003
UT1	FORS1	600V	4.9	4830 – 7200	Mar–Aug 2003

<sup>a</sup>Unvignetted part of spectrum

Table 2. Target List, Exposure Times and QSO Redshift Coverage

QSO	$z_{\text{em}}$	$B$ mag. <sup>a</sup>	Telescope	Exposure Time (s)	$\Delta z > 0.3\text{\AA}^{\text{b}}$	$\Delta z > 0.6\text{\AA}^{\text{b}}$	$\Delta z > 1.0\text{\AA}^{\text{b}}$
B0039-407	2.478	19.7	3.6	2700	0.0114	0.5494	0.7135
B0048-071	1.975	21.4	WHT	10800	1.0805	1.1602	1.1721
B0104-275	2.492	19.3	3.6	2700	0.0242	0.7134	0.7155
B0106+013	2.094	18.6	WHT	3000	1.0574	1.1593	1.1671
B0122-005	2.280	18.5	WHT	3600	1.1444	1.1722	1.1750
B0136-059	2.004	21.4	VLT	4000	0.0000	0.2306	0.8376
B0136-231	1.893	18.3	3.6	2000	0.7135	0.7171	0.7171
B0226-038	2.064	17.9	WHT	3600	1.1678	1.1760	1.1763
B0227-369	2.115	19.6	3.6	5400	0.0000	0.0810	0.7120
B0234-301	2.102	18.1	3.6	1800	0.0171	0.7134	0.7155
B0240-060	1.805	18.7	WHT	3600	1.1356	1.1665	1.1719
B0244-128	2.201	18.4	WHT	3600	0.6603	1.1520	1.1668
B0254-334	1.915	19.2	3.6	3600	0.0000	0.2637	0.7143
B0256-005	1.998	17.3	WHT	2800	1.1112	1.1657	1.1719
B0325-222	2.220	19.0	3.6	1800	0.0000	0.2445	0.7107
B0420+022	2.277	20.2	WHT	14400	1.1410	1.1688	1.1738
B0421+019	2.048	17.3	WHT	3600	1.1429	1.1710	1.1751
B0422-389	2.346	18.4	3.6	2700	0.0227	0.7099	0.7163
B0436-203	2.146	22.8 <sup>†</sup>	...	...	...	...	...
B0440-285	1.952	18.4	3.6	2700	0.5991	0.7150	0.7171
B0446-212	1.971	18.7	3.6	2400	0.0057	0.7141	0.7170
B0448-187	2.050	20.2	Baade	3600	0.8149	1.1251	1.1351
B0458-020	2.286	19.0	WHT	5400	0.2295	1.0163	1.1430
B0524-433	2.164	18.0 <sup>†</sup>	3.6	3600	0.0078	0.0953	0.6995
B0606-223	1.926	20.0 <sup>†</sup>	Baade	6000	1.1350	1.1350	1.1350
B0618-252	1.900	18.2 <sup>†</sup>	3.6	3600	0.7035	0.7170	0.7170
B0642-349	2.165	18.5 <sup>†</sup>	3.6	2600	0.3439	0.7106	0.7141
B0805-077	1.837	19.0 <sup>†</sup>	WHT	3600	0.8451	0.8458	0.8458
B0819-032	2.352	19.4	WHT	7200	0.1699	0.8352	0.8420
B0919-260	2.300	19.0 <sup>†</sup>	3.6	3600	0.7056	0.7141	0.7141

Table 2—Continued

QSO	$z_{\text{em}}$	$B$ mag. <sup>a</sup>	Telescope	Exposure Time (s)	$\Delta z > 0.3\text{\AA}^{\text{b}}$	$\Delta z > 0.6\text{\AA}^{\text{b}}$	$\Delta z > 1.0\text{\AA}^{\text{b}}$
B0945-321	2.140	19.0 <sup>†</sup>	3.6	3600	0.0000	0.7024	0.7116
B1005-333	1.837	18.0 <sup>†</sup>	3.6	1800	0.0000	0.5197	0.7113
B1022-102	2.000	16.8 <sup>†</sup>	WHT	3600	0.8432	0.8459	0.8459
B1032-199	2.198	18.2	WHT	5400	0.2719	0.8377	0.8412
B1034-374	1.821	18.5 <sup>†</sup>	3.6	2600	0.0000	0.6351	0.7070
B1055-301	2.523	19.3	Baade	3600	1.0787	1.1350	1.1350
B1106-227	1.875	20.3	Baade	4500	1.0173	1.1333	1.1350
B1117-270	1.881	19.0 <sup>†</sup>	3.6	3600	0.0590	0.7088	0.7131
B1143-245	1.940	18.1	3.6	1800	0.5703	0.7120	0.7141
B1147-192	2.489	20.3	Baade	3500	0.0245	0.3658	1.0166
B1148-001	1.978	17.4	WHT	2400	0.8433	0.8459	0.8459
B1149-084	2.370	20.0	VLT	1800	0.8377	0.8465	0.8485
B1228-310	2.276	19.8	3.6	5400	0.0000	0.5197	0.7056
B1230-101	2.394	19.6	Baade	2700	0.0446	1.0363	1.1344
B1255-316	1.924	18.3	3.6	2600	0.2506	0.7127	0.7141
B1256-177	1.956	21.4	VLT	1800	0.8464	0.8480	0.8480
B1256-243	2.263	19.4	3.6	5400	0.6277	0.7131	0.7131
B1318-263	2.027	21.3	VLT	4000	0.4884	0.8393	0.8439
B1319-093	1.864	19.6	WHT	9000	0.6455	0.8396	0.8426
B1324-047	1.882	19.8	WHT	9000	0.1574	0.8366	0.8407
B1402-012	2.518	18.0	WHT	2400	0.8404	0.8457	0.8459
B1406-267	2.430	21.8 <sup>†</sup>	VLT	7200	0.7351	0.8435	0.8485
B1412-096	2.001	17.4	WHT	6000	0.2278	0.8328	0.8420
B1422-250	1.884	19.6 <sup>†</sup>	3.6	5400	0.0178	0.7017	0.7095
B1430-178	2.331	19.4	3.6	3600	0.1905	0.7131	0.7131
B1451-400	1.810	18.5 <sup>†</sup>	3.6	2600	0.0000	0.3980	0.7113
B1550-269	2.145	21.0 <sup>†</sup>	VLT	3000	0.8404	0.8470	0.8487
B1654-020	2.000	23.5 <sup>†</sup>	...	...	...	...	...
B1657+022	2.039	19.2	WHT	6900	0.8126	0.8430	0.8449
B2044-168	1.943	18.0	WHT	3600	1.1667	1.1752	1.1755

Table 2—Continued

QSO	$z_{\text{em}}$	$B$ mag. <sup>a</sup>	Telescope	Exposure Time (s)	$\Delta z > 0.3\text{\AA}^{\text{b}}$	$\Delta z > 0.6\text{\AA}^{\text{b}}$	$\Delta z > 1.0\text{\AA}^{\text{b}}$
B2123-015	2.196	19.9 <sup>†</sup>	VLT	5000	0.0075	0.7955	0.8391
B2134+004	1.936	17.2	WHT	3600	1.1651	1.1727	1.1746
B2145-176	2.130	20.1	VLT	1600	0.0981	0.8395	0.8445
B2149-307	2.345	18.4	3.6	2700	0.7155	0.7170	0.7170
B2200-238	2.118	18.0	3.6	1800	0.2153	0.7171	0.7171
B2210-257	1.833	18.5	3.6	2700	0.0000	0.7134	0.7163
B2217-011	1.878	20.4 <sup>†</sup>	VLT	5400	0.0278	0.8362	0.8437
B2224+006	2.248	22.0	VLT	7200	0.4198	0.8424	0.8466
B2245-128	1.892	18.3	WHT	3600	1.0310	1.1588	1.1686
B2245-328	2.268	18.3	3.6	2700	0.0590	0.7150	0.7171
B2254+024	2.090	17.8	WHT	3600	1.1570	1.1718	1.1749
B2311-373	2.476	18.4	3.6	2700	0.0732	0.7135	0.7171
B2314-409	2.448	19.0	3.6	1950	0.4775	0.7155	0.7170
B2315-172	2.462	21.0	VLT	2500	0.0133	0.1155	0.8424
B2325-150	2.465	20.0	VLT	1200	0.2600	0.8474	0.8482

<sup>a</sup> $B$  band magnitudes from the APM catalogue (accurate to approximately 0.3 magnitudes), except those marked with a † which are from Jackson et al. (2002)

<sup>b</sup>Redshift coverage based on a given EW detection threshold at  $5\sigma$  significance.

Table 3. Mg II  $\lambda$ 2796 and Fe II  $\lambda$ 2600 Absorption Line  
Catalogue and Rest Frame Equivalent Widths

QSO	$z_{\text{abs}}$	$W_0(\text{Mg II } \lambda 2796)$ ( $\text{\AA}$ )	$W_0(\text{Fe II } \lambda 2600)$ ( $\text{\AA}$ ) <sup>a</sup>
B0039-407	0.8483	$2.35 \pm 0.15$	$2.09 \pm 0.22$
B0048-071	1.4919	$0.90 \pm 0.03$	$0.36 \pm 0.04$
B0048-071	1.5698	$0.32 \pm 0.03$	$<0.07$
B0106+013	1.4256	$0.47 \pm 0.04$	$0.22 \pm 0.05$
B0122-005	0.9949	$1.56 \pm 2.08$	$0.56 \pm 0.38$
B0122-005	0.9973	$0.23 \pm 0.05$	$<0.07$
B0136-231	0.8020	$0.44 \pm 0.06$	...
B0136-231	1.1832	$0.68 \pm 0.06$	$0.27 \pm 0.07$
B0136-231	1.2937	$0.75 \pm 0.06$	$0.23 \pm 0.06$
B0226-038	1.3284	$0.70 \pm 0.02$	$<0.37$
B0227-369	1.0289	$0.59 \pm 0.18$	$0.61 \pm 0.16$
B0234-301	0.8238	$0.91 \pm 0.11$	$0.27 \pm 0.20$
B0240-060	0.5810	$1.44 \pm 0.08$	...
B0240-060	0.7550	$1.65 \pm 0.04$	$1.25 \pm 0.04$
B0240-060	1.6310	$0.34 \pm 0.03$	$<0.06$
B0244-128	0.8282	$1.77 \pm 0.09$	$1.23 \pm 0.09$
B0244-128	1.2215	$0.57 \pm 0.11$	$0.36 \pm 0.10$
B0254-334	1.1192	$0.81 \pm 0.19$	$<0.25$
B0256-005	1.3369	$1.70 \pm 0.43$	$0.31 \pm 0.12$
B0256-005	1.6134	$0.25 \pm 0.04$	$<0.07$
B0420+022	0.9490	$0.25 \pm 0.05$	$<0.07$
B0421+019	0.7394	$0.48 \pm 0.09$	$<0.11$
B0421+019	1.6379	$0.28 \pm 0.03$	$<0.07$
B0422-389	1.2956	$0.62 \pm 0.11$	$<0.28$
B0458-020	0.8904	$0.65 \pm 0.12$	$<0.27$
B0458-020	1.5271	$2.09 \pm 0.82$	$0.44 \pm 0.13$
B0458-020	1.5605	$0.94 \pm 0.08$	$0.75 \pm 0.08$
B0606-223	0.5078	$0.25 \pm 0.04$	...
B0606-223	0.8959	$0.55 \pm 0.02$	$0.41 \pm 0.03$
B0606-223	0.9343	$0.23 \pm 0.02$	$<0.06$

Table 3—Continued

QSO	$z_{\text{abs}}$	$W_0(\text{Mg II } \lambda 2796)$ ( $\text{\AA}$ )	$W_0(\text{Fe II } \lambda 2600)$ ( $\text{\AA}$ ) <sup>a</sup>
B0606-223	1.2443	$1.40 \pm 0.04$	$1.07 \pm 0.04$
B0606-223	1.5313	$1.55 \pm 0.07$	$1.27 \pm 0.05$
B0919-260	0.7048	$0.81 \pm 0.08$	...
B0919-260	0.7626	$0.35 \pm 0.07$	...
B0945-321	1.1702	$0.91 \pm 0.12$	$<0.26$
B1005-333	1.3734	$0.93 \pm 0.10$	$0.84 \pm 0.11$
B1022-102	0.7141	$0.34 \pm 0.03$	$<0.08$
B1022-102	1.3085	$0.17 \pm 0.03$	...
B1148-001	1.2450	$0.31 \pm 0.05$	$<0.11$
B1148-001	1.4671	$0.22 \pm 0.03$	$0.10 \pm 0.04$
B1230-101	0.7472	$2.10 \pm 0.15$	$<1.33$
B1230-101	0.7810	$0.86 \pm 0.10$	$<0.26$
B1255-316	0.6923	$0.34 \pm 0.10$	...
B1256-177	0.9399	$2.96 \pm 0.04$	$2.08 \pm 0.04$
B1256-177	1.3667	$1.28 \pm 0.03$	$0.33 \pm 0.03$
B1256-177	1.5035	$0.26 \pm 0.03$	$<0.08$
B1318-263	1.1080	$1.38 \pm 0.08$	$0.61 \pm 0.07$
B1324-047	0.7850	$2.58 \pm 0.12$	$1.77 \pm 0.11$
B1402-012	0.8901	$1.21 \pm 0.04$	$0.99 \pm 0.04$
B1412-096	1.3464	$0.66 \pm 0.11$	...
B1430-178	1.3269	$0.60 \pm 0.08$	$0.45 \pm 0.07$
B1451-400	0.9330	$0.71 \pm 0.18$	$<0.42$
B2044-168	0.8341	$0.23 \pm 0.03$	$<0.06$
B2044-168	1.3287	$0.59 \pm 0.02$	$<0.14$
B2149-307	1.0904	$1.45 \pm 0.04$	$0.78 \pm 0.04$
B2245-128	0.5869	$1.28 \pm 0.08$	...
B2314-409	1.0439	$0.39 \pm 0.08$	$<0.21$



<sup>a</sup> '...' indicates that the transition was not covered

Table 4. Redshift Path for Complete QSO Sample for Various Detection Thresholds

Coverage	0.3 Å	0.5 Å	0.6 Å	1.0 Å
3 $\sigma$ Mg II only	54.05	63.38	63.77	64.19
5 $\sigma$ Mg II only	35.15	54.05	58.24	63.77
3 $\sigma$ Mg II and Fe II	44.62	53.51	53.85	55.10
5 $\sigma$ Mg II and Fe II	28.11	44.62	48.52	53.85

Table 5. Number of Systems, Mean Redshift, and Redshift Path for the RT00, SS92 and CORALS Samples at 5 $\sigma$  significance.

$W_{min}$ (Å)	RT00			SS92			CORALS II		
	$N_{MgII}$	$\langle z \rangle$	$\Delta z$	$N_{MgII}$	$\langle z \rangle$	$\Delta z$	$N_{MgII}$	$\langle z \rangle$	$\Delta z$
0.3	87	0.83	104.6	111	1.12	114.2	45	1.09	35.15
0.6	44	0.83	103.7	67	1.17	129.0	32	1.09	58.24
1.0	...	...	...	...	...	...	17	1.01	63.77

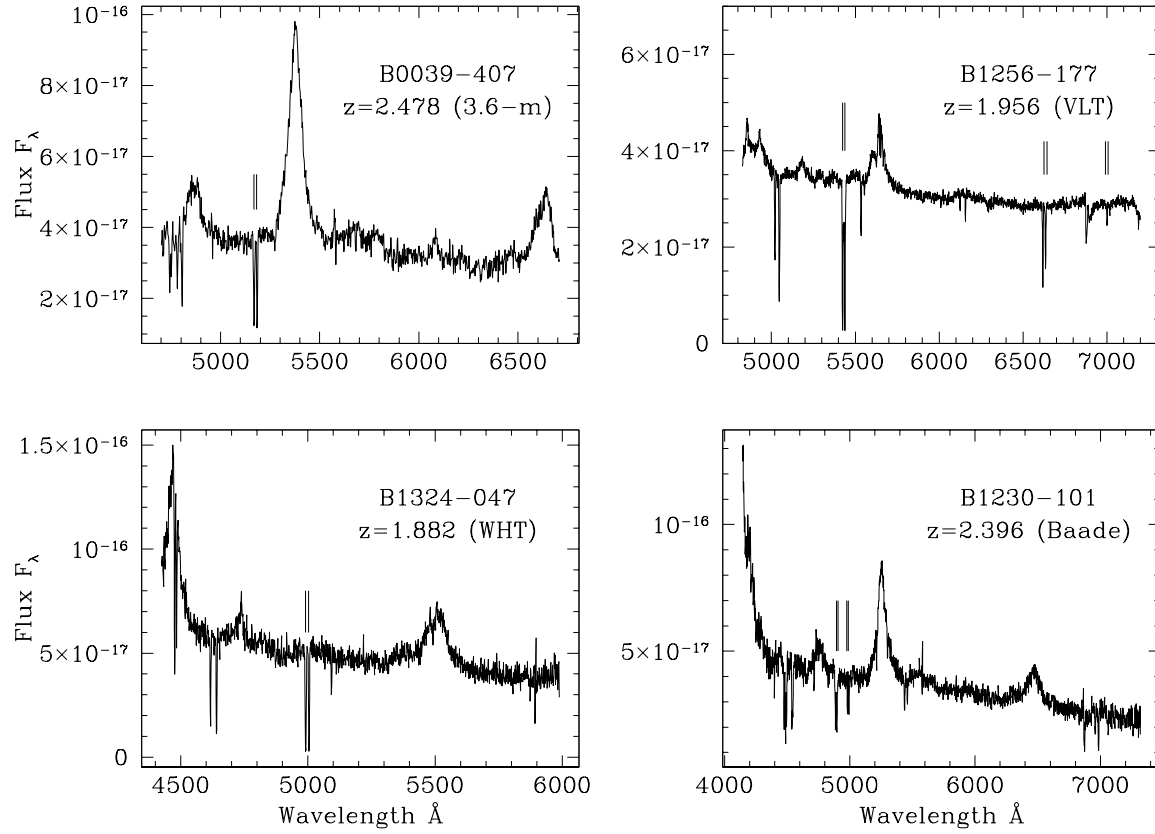


Fig. 1.— Examples of spectra obtained with the four telescopes utilized for this program. Mg II systems listed in Table 3 are indicated with vertical tick marks.

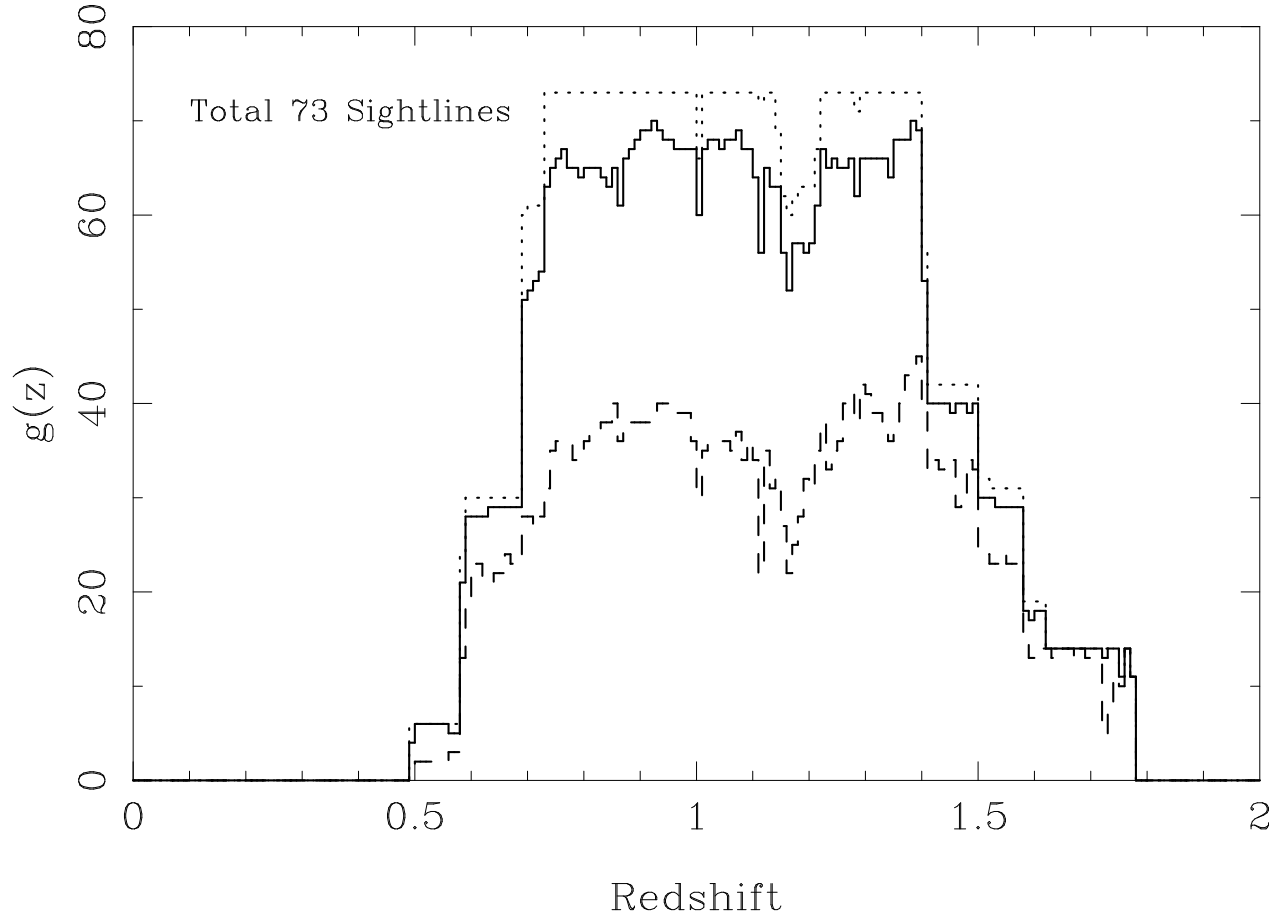


Fig. 2.— The redshift path density,  $g(EW_{min}, z_i)$  for three minimum EW limits, as a function of redshift. Dotted, solid and dashed lines are 1.0, 0.6 and 0.3Å (at  $5\sigma$  significance) respectively.

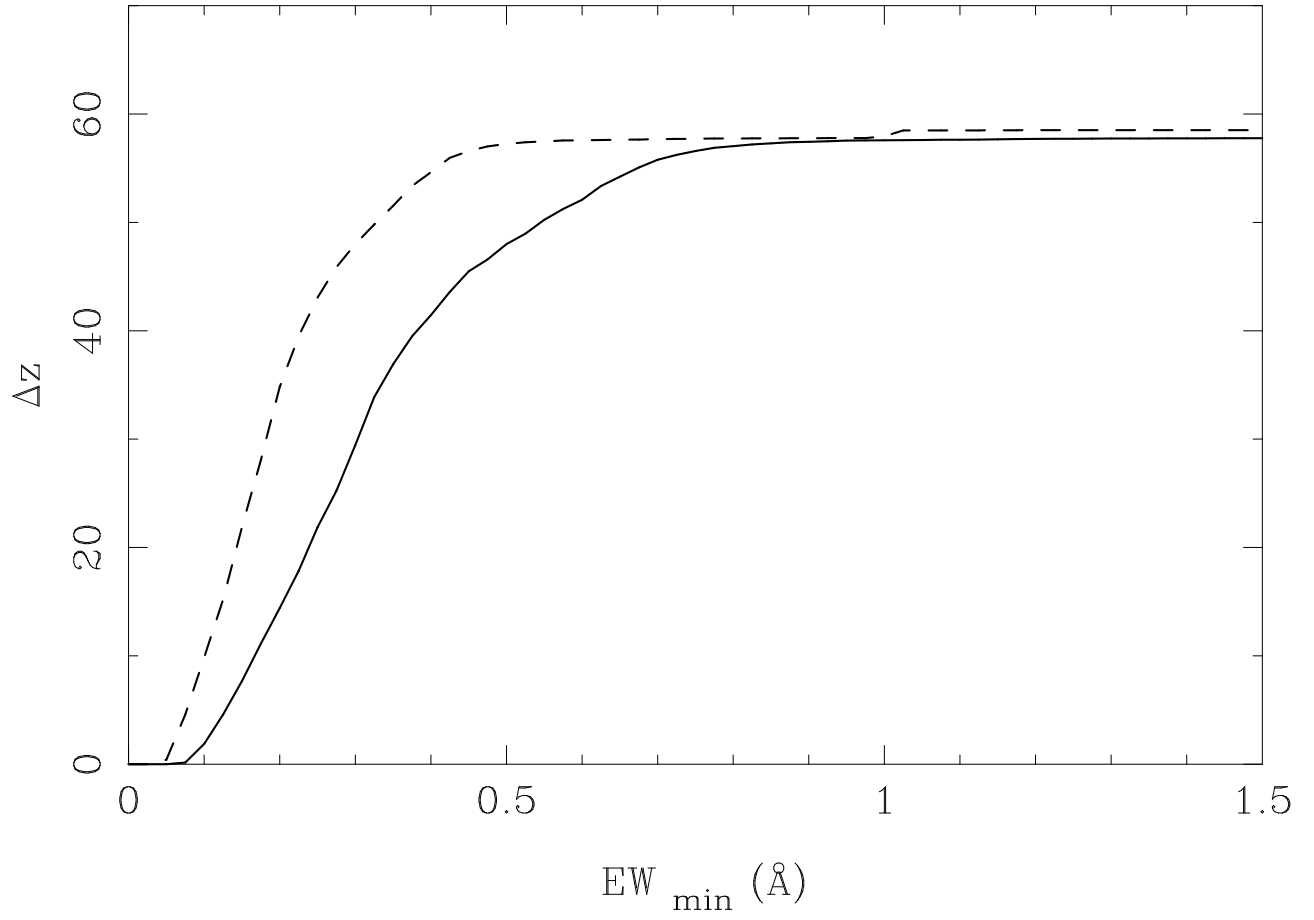


Fig. 3.— The cumulative redshift path ( $\Delta z$ ) covered as a function of rest frame EW. The solid line is for  $5\sigma$ , dashed is  $3\sigma$ .

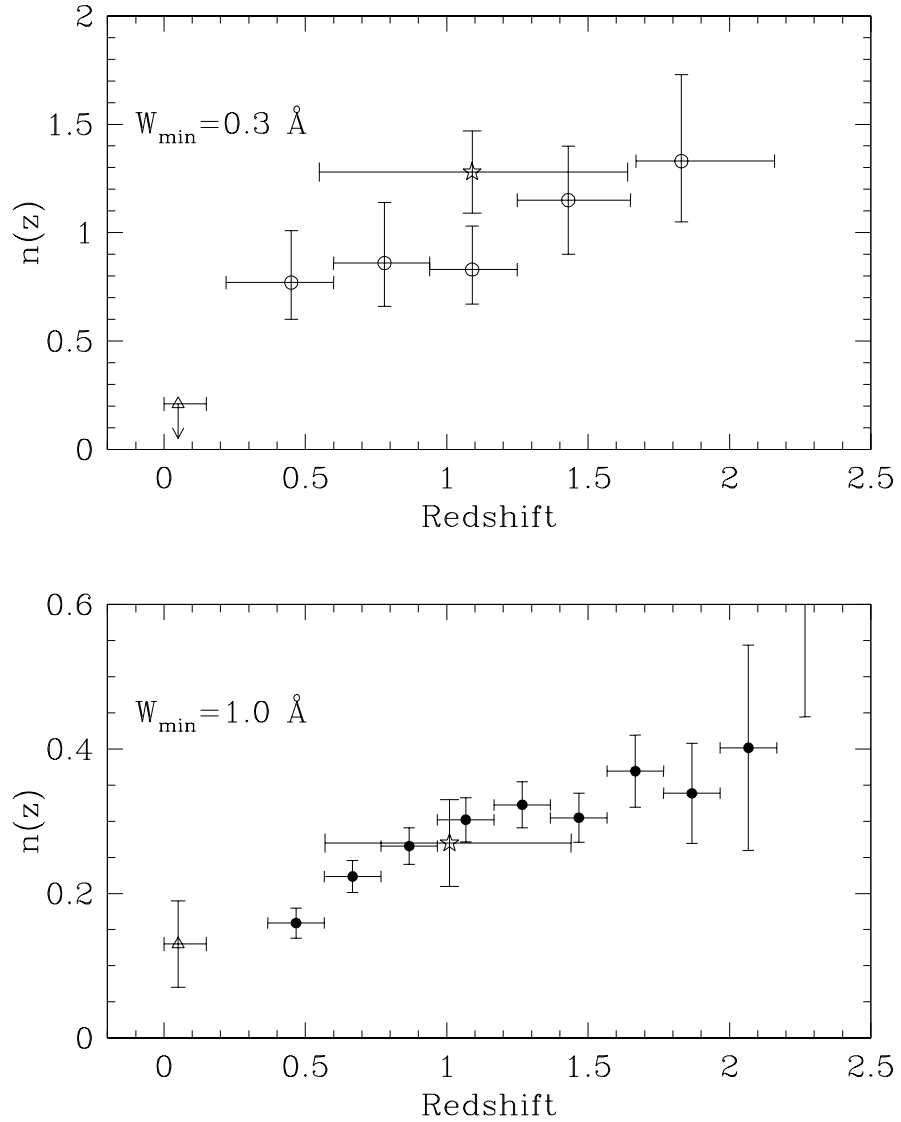


Fig. 4.— The number density of Mg II systems,  $n(z)$ , in the CORALS II survey (open stars) compared with Steidel & Sargent (1992), preliminary results from the SDSS EDR (Nestor et al. 2003a) and Churchill (2001) which are plotted with open circles, solid circles and open triangles respectively. Results are shown for two minimum EW thresholds.

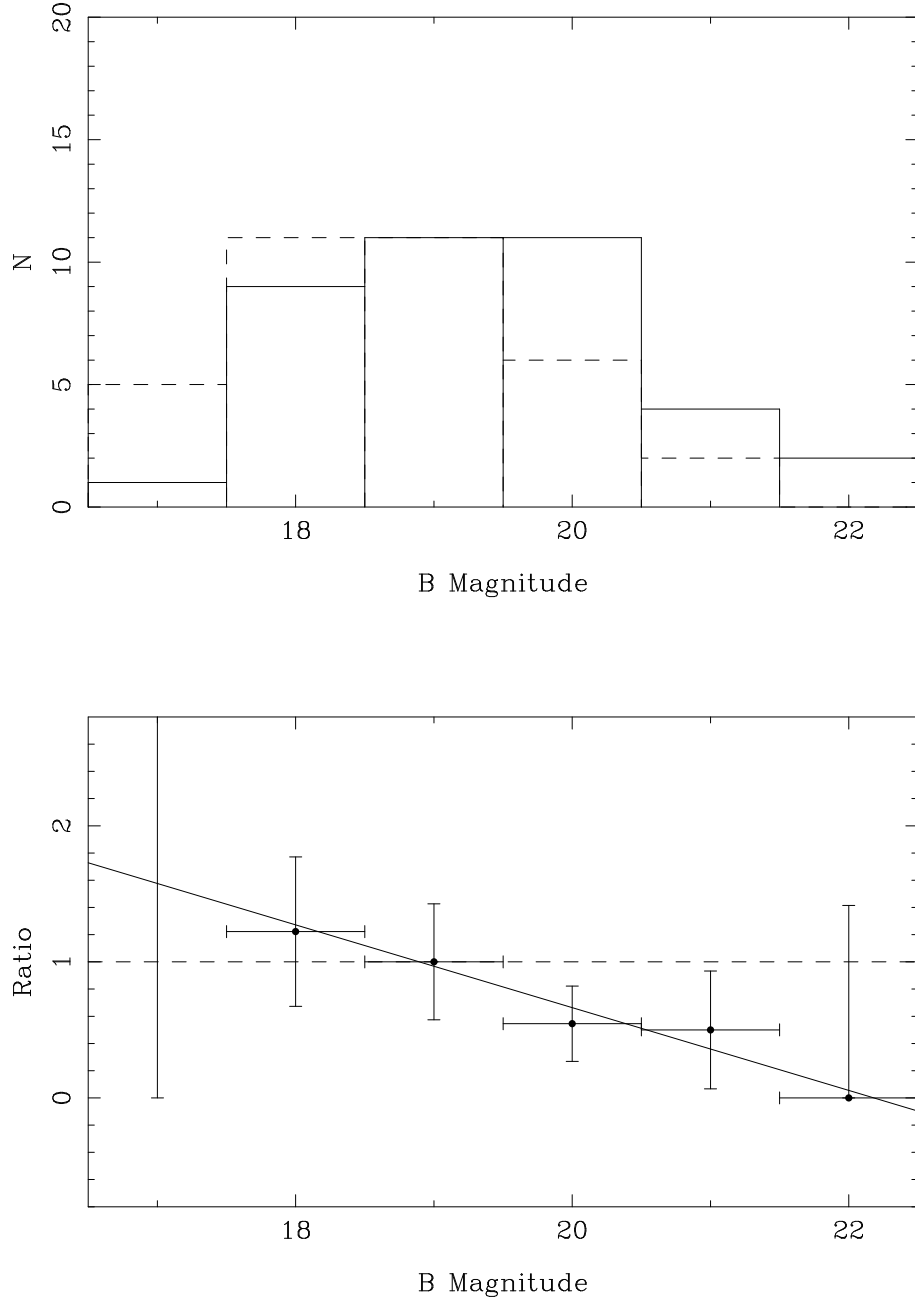


Fig. 5.— Top:  $B$ -band magnitude distributions for QSOs with (dashed line) and without (solid line) intervening Mg II systems. All Mg II systems in Table 3 are included. Bottom: The ratio of the number of QSOs with:without intervening systems in each magnitude bin from the top panel. There is a small excess of  $B \lesssim 19$  QSOs with absorbers compared with fainter targets. The solid line shows a least squares fit to these ratios (excluding the point at  $B = 17$ ) with a slope of  $-0.3$ . The dashed horizontal line shows a ratio of one.

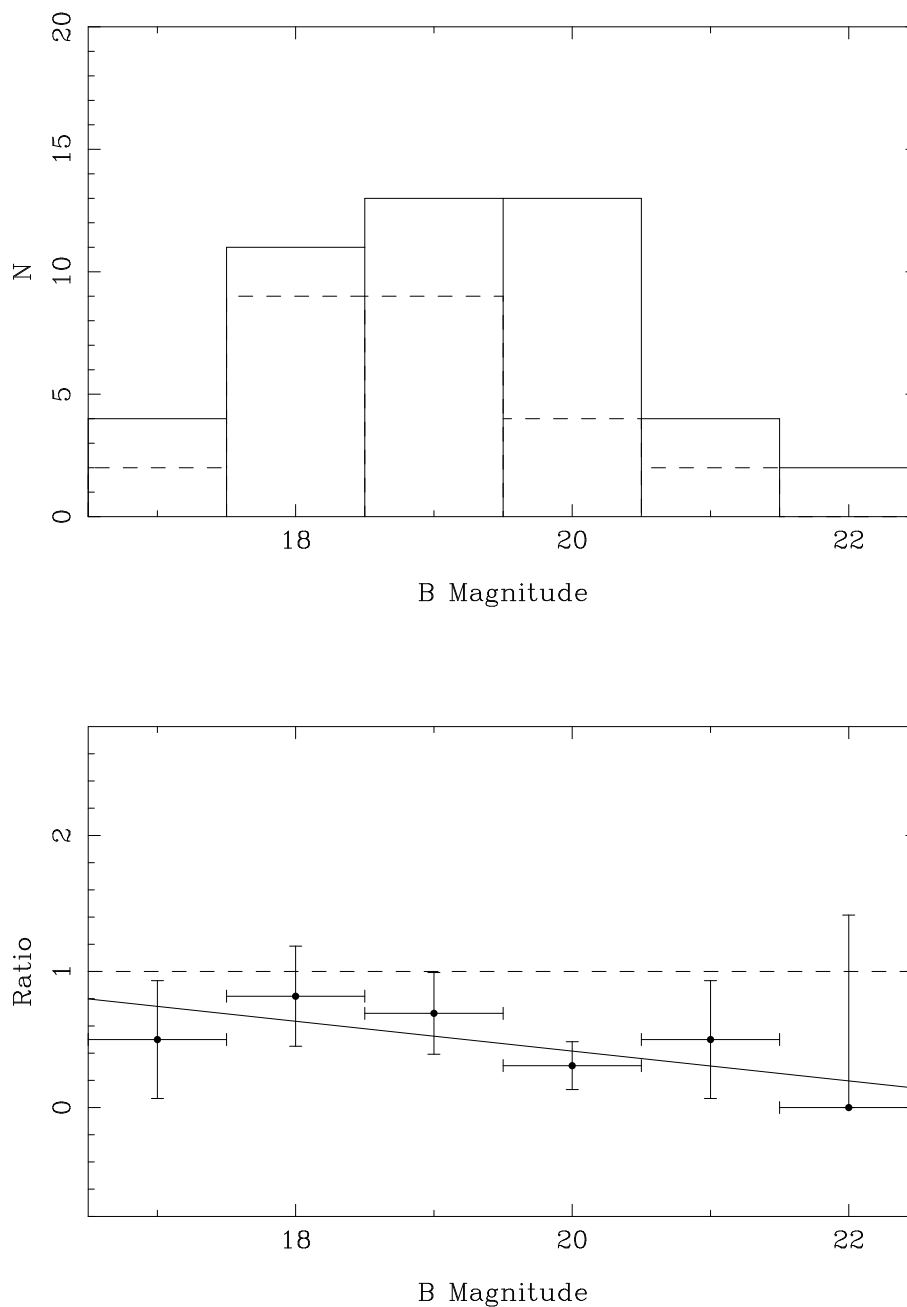


Fig. 6.— Top:  $B$ -band magnitude distributions for QSOs with (dashed line) and without (solid line) intervening Mg II systems with  $EW \geq 0.6 \text{ \AA}$ . Bottom: The ratio of the number of QSOs with:without intervening systems in each magnitude bin from the top panel. The solid line shows a least squares fit to these ratios with a slope of  $-0.1$  and the dashed horizontal line shows a ratio of one. This figure is analogous to Figure 5 except that the EW cut-off ensures completeness in our absorption system selection.



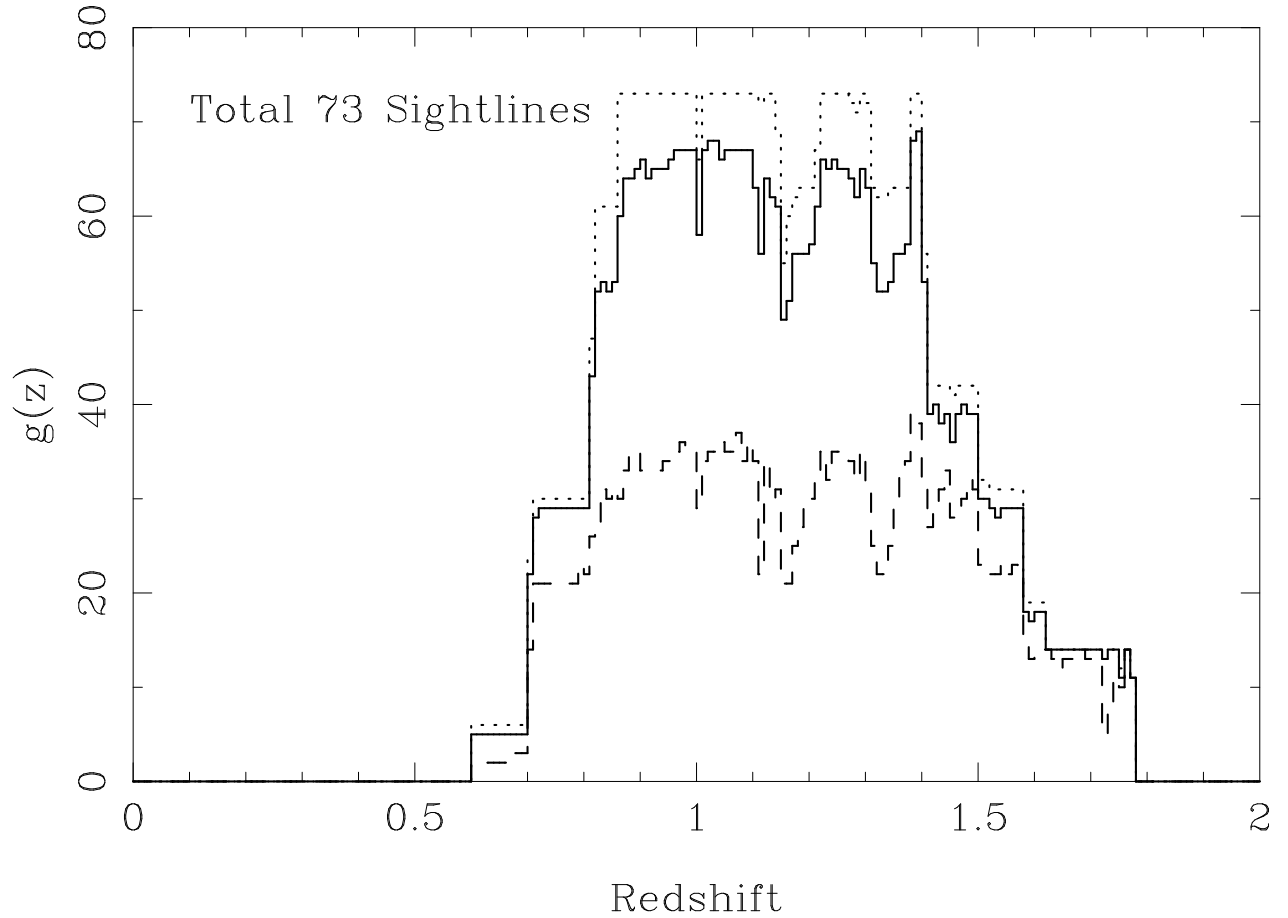


Fig. 7.— The redshift path density,  $g(EW_{min}, z_i)$  for three minimum EW limits of both Mg II and Fe II, as a function of redshift. Dotted, solid and dashed lines are for EW limits of 1.0, 0.6 and 0.3 Å (at  $5\sigma$  significance) respectively.

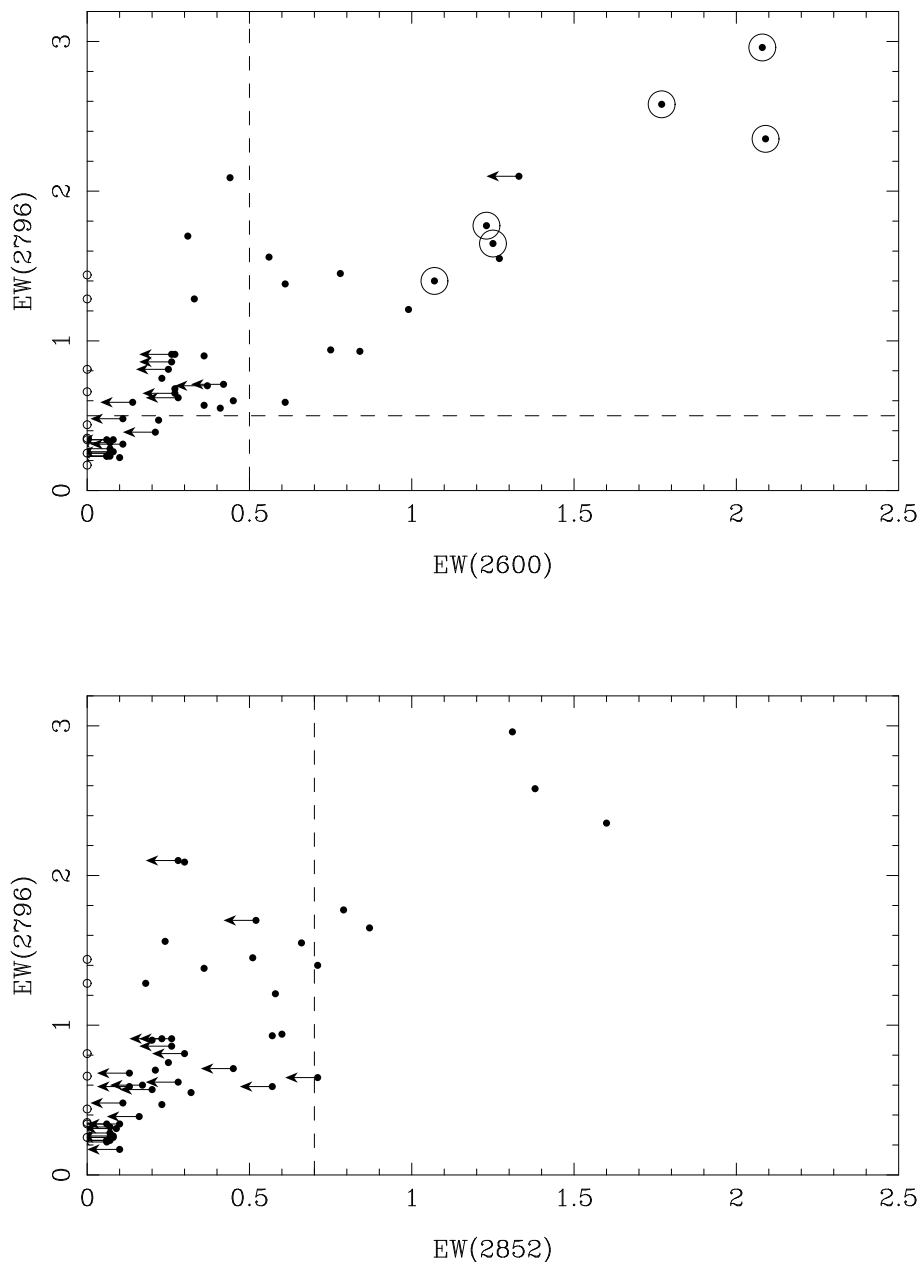


Fig. 8.— Top panel: Comparison of Mg II and Fe II EWs. DLA candidates can be selected from absorbers that have rest equivalent widths of Mg II $\lambda$ 2796 and Fe II $\lambda$ 2600 greater than 0.5 Å (dashed lines). Solid points surrounded with large open circles are systems with EW(Mg I  $\lambda$ 2852) > 0.7 Å. Small open points along the y axis indicate that Fe II $\lambda$ 2600 was not covered in the spectrum. Bottom panel: Comparison of Mg II and Mg I EWs; symbols as for upper panel. RT00 found that all systems with EW(Mg I $\lambda$ 2852) > 0.7 Å were confirmed to be DLAs (dashed line).

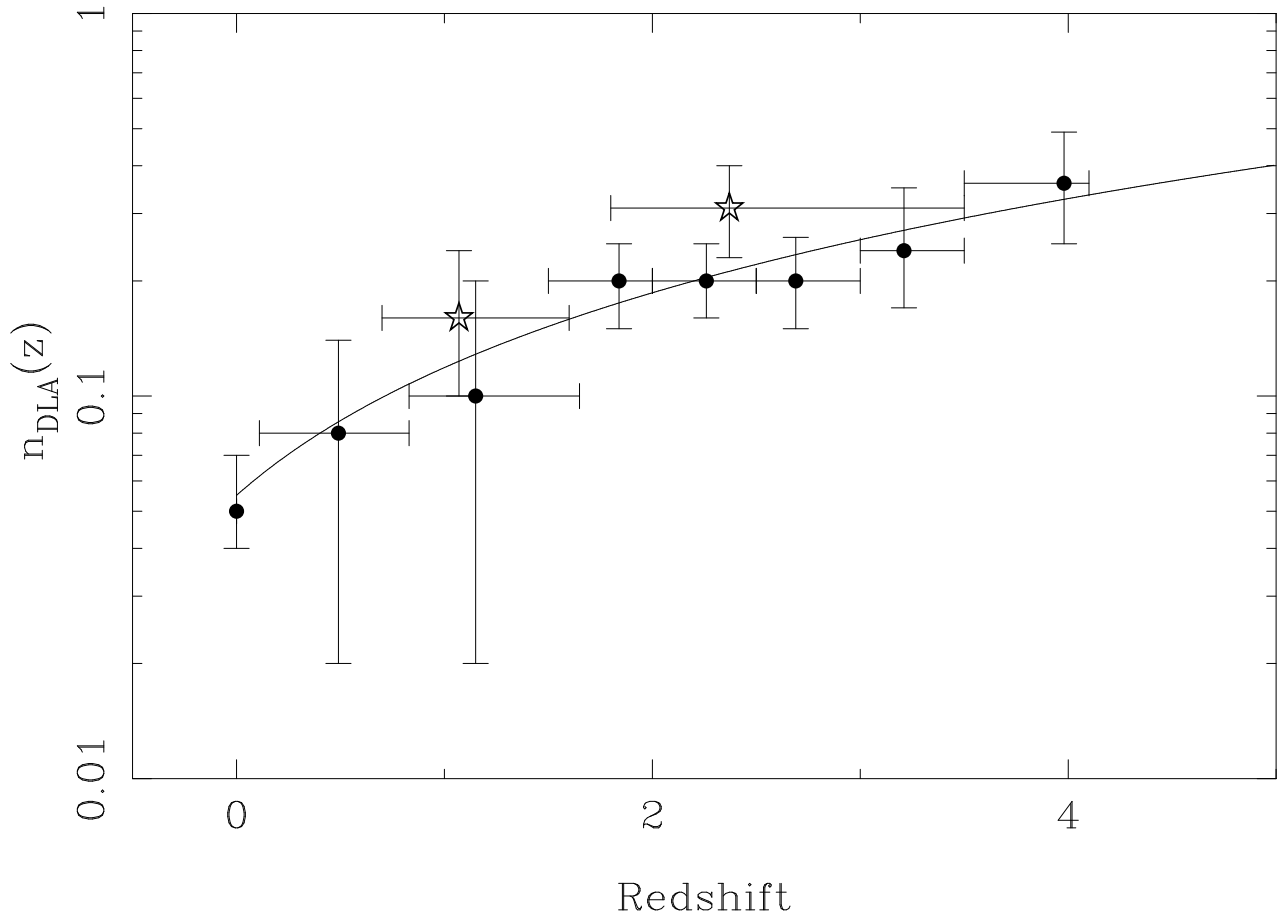


Fig. 9.— The number density of DLAs as a function of redshift. Solid points taken from the literature are from Rosenberg & Schneider (2003), Rao & Turnshek (2000) and Storrie-Lombardi & Wolfe (2000) for  $z=0$ ,  $0.1 < z < 1.65$  and  $z > 1.5$  respectively. . The open stars are the values inferred for the high (Ellison et al 2001) and low (this work) redshift CORALS surveys. All error bars are  $1 \sigma$  based on Gehrels (1986) except for the  $z = 0$  point where the error is as quoted by Rosenberg & Schneider (2003). The solid line shows the fit of Storrie-Lombardi & Wolfe (2000):  $n(z) = 0.055(1 + z)^{1.11}$ .